I never received reprint of this one.

Vannada Lectures

in Solid State Astrophysics ed Bussoletti & Strazzulla (1991) (N. Holland) 29

NASA-TM-112460

NDB 7N-90-TM 027660

Laboratory, Observational, and Theoretical Studies of Interstellar Ices

A.G.G.M. Tielens, L.J. Allamandola, and S. A. Sandford
NASA Ames Research Center,
MS 245-6, Moffett Field,
CA 94035, USA.

I Introduction

The application of spectroscopic studies of gaseous species (atoms, ions, and molecules) to the interpretation of astronomical spectra dates back to the previous century. The parallel approach to the study of interstellar dust is, however, rather recent. Although the existence of interstellar dust was recognized in the 1930's (1), laboratory studies of dust analogs have begun only recently, with the first serious attempts in the 1960's (2). Even with this, the effort devoted to dust has been much less than that devoted to the gas phase. This situation has recently changed due to the development of sophisticated ground-, air-, and space-based observational techniques, especially in the infrared. To fully exploit these new observations it has become necessary to study laboratory analogs.

One of the most active areas of laboratory work has been the study of the properties of various mixed ices of astrophysical interest. For example, particle bombardment experiments on ice samples have been made to investigate the effects of sputtering and ion-chemistry by solar wind and cosmic ray irradiation (3-7). Similar studies have been made using ultraviolet photons instead of ions (8-11). Many of these studies utilized spectroscopic techniques to analyze the results. General reviews of this emerging field have appeared over the last decade (2,12,13). Some

references which contain detailed quantitative spectroscopic information on astrophysically relevant ices are: (14-19). While not exhaustive, the references listed above and references therein provide a good overview of the work in this field.

This paper presents an overview of our current understanding of interstellar ices. It borrows heavily from several reviews that we have published previously (12,13,20-22). In §II the chemistry of interstellar icy grain mantles is discussed. Besides a review of theoretical calculations of grain surface chemistry occuring upon accretion, it also summarizes the results of various laboratory experiments on the effects of UV irradiation on ices. After a brief description of the basic laboratory techniques involved in (interstellar) ice analog studies (§III), the fundamentals of infrared spectroscopy are reviewed (§IV) with an emphasis on solid state effects. This is then illustrated with an analysis of the spectrum of H_2O ice and a quantitative description of column density determinations. The observed composition of interstellar ices derived from IR observations of protostars embedded inside dense clouds is then discussed and compared to the results of theoretical calculations (§V). Finally, §VI present a summary of this paper.

II Icy Grain Mantles in Dense Molecular Clouds

Dense interstellar clouds are comprised of gas and dust. The gas is a mixture of many different atomic and molecular species. During the past three decades radio astronomers have discovered more than fifty interstellar polyatomic molecules in these clouds (23). Interspersed with the gas, at much lower abundance ($\approx 10^{-12}$ per H atom), are small ($\approx$1000Å), cold ($\approx$10 K) dust particles. Because the grains are cold, most gaseous species (except H, He, and H_2) striking the grains will stick, forming a mixed molecular ice mantle. The accreting atoms, radicals, and molecules may react with each other. At this point in our understanding of chemistry in clouds, two general classes of molecular mantle are envisioned. One class is comprised largely of relatively simple species

formed by grain surface reactions. The other consists of a chemically more complex mixture resulting from UV photolysis of this simple mixture (Fig. 1). These are often called "icy" grain mantles and organic refractory grain mantles, respectively, in the literature. They will be discussed in turn in the remainder of this section.

A) Grain Surface Chemistry

Gas phase species colliding with cold (≈10K), interstellar grains are expected to stick to the surface with almost unit probability (20). Although the flux of incoming species is typically very low (few/day), all heavy gas phase species should have accreted in about 10^5 yrs at a density of 10^4 cm^{-3}. Since some of the accreted species will be mobile (i.e., atomic H and O) on such surfaces, reactions between them, as well as with immobile species, are important and will lead to the formation of a molecular grain mantle whose composition may be quite different from the gas phase (24-27). This is illustrated in Fig. 2 which compares the calculated gas phase and grain mantle composition of interstellar clouds as a function of total gas phase density.

In the gas phase, hydrogen is mainly in the form of H_2, carbon in the form of CO, nitrogen and the remainder of the oxygen are either in atomic (N, O) or diatomic (N_2, O_2) form, depending on the physical conditions (Fig. 2). At low densities atomic H is an important constituent of the gas phase and it dominates the grain surface reactions. Under such reducing conditions, hydrides such as H_2O and H_2CO formed from O, O_2, and CO are calculated to be abundant grain mantle species (Fig. 2). Note that the grain mantle abundance of NH_3 is low since most of the elemental N in the gas phase is in the form of N_2 and its reaction with H is inhibited by a large activation barrier. Likewise, little CH_4 is formed since most of the elemental C is in the form of CO. In these calculations, reduction of CO was stopped at H_2CO. Recent laboratory experiments suggest that the H addition to H_2CO has a low activation energy (28) and most of the H_2CO in the grain mantles might actually be reduced to CH_3OH.

At high densities, the gas phase abundance of heavy species is much larger than that of atomic H and as a result the composition of the grain mantle will be quite different. When atomic O has a low gas-phase abundance, few grain surface reactions will occur and an inert grain mantle will result, consisting mainly of CO and O_2 (Fig. 2), which reflects their gas phase dominance. However, if the gas phase O abundance is high, CO may be oxidized to CO_2. It has been suggested that this reaction is inhibited at low temperatures by an activation barrier (29). However, while O atoms can be stored in a CO matrix at 10 K, CO_2 is formed immediately when the matrix is warmed (30). The reaction seems therefore to be mainly inhibited by steric factors rather than an activation barrier. Steric factors are probably less important on a grain surface than in a matrix and CO_2 might be an important grain mantle constituent under these conditions. Further experimental studies are important to better determine the kinetics of this reaction at low temperatures.

Grain surface reactions can also lead to large deuteration effects (Fig. 2; 25,27). The D and H grain surface reaction networks are very similar and this deuteration directly reflects the high gas phase D to H ratio ($> 10^{-2}$), which is much larger than the elemental abundance ratio ($\approx 10^{-5}$). This is a direct consequence of ion-molecule gas phase chemistry which produce high abundances of deuterated ions (i.e., DCO^+), that dissociatively recombine with electrons to form atomic D (25,31).

In summary, theoretical calculations predict that grain surface chemistry can produce three different components of icy grain mantles in molecular clouds depending on the physical conditions in the gas phase. They are: 1) a reduced component (i.e., H_2O and CH_3OH); 2) an inert component (i.e., CO and O_2); and 3) an oxidized component (i.e., CO_2). Although in any given region one component will be dominant, along a line of sight multiple components may be present. Another characteristic of grain surface reactions is large deuterium fractionation of hydrides.

B UV photolysis of icy grain mantles

Significantly more complex ice mantles should be produced by energetic processing with ultraviolet radiation and cosmic rays (3,32). The products of irradiation span a broad range in complexity, starting with molecules as "simple" as CO_2 and H_2CO, and extending to large, poorly characterized "polymers" (20). UV photolysis of simple molecular ices produces reactive radicals (such as H, O, and OH), often in electronic or vibrationally excited states. These radicals can react with their neighbors or diffuse through the ice and react with other species present. Because of the large amount of excess energy available, even reactions with molecules having closed electronic shells, which normally have appreciable activation barriers, become possible. An example of the possible reaction pathways involving CO and the simple photoproducts of an ice made of H_2O, CH_4, and NH_3 is shown in Fig. 3. Note how even a few steps are sufficient to produce complex molecules, such as acetaldehyde (CH_3CHO).

Since the diffusing radicals may lose most of their excess energy through collisions with matrix molecules before finding a reaction partner, they can also be stored at low temperatures in interstitial or substitutional sites. Upon warm-up above 30K these radicals can diffuse again and react, forming more complex molecules and resulting in a so-called organic refractory grain mantle (9,32-34). Whether this actually takes place inside dense interstellar clouds depends on two conditions: 1) The presence of an internal UV source; and 2) the presence of a (transient) heating mechanism for grain mantles (20). Cosmic rays may play a major role for both conditions. Cosmic ray excitation of H_2 molecules leads to UV fluorescence in the Lyman-Werner bands, resulting in an average UV field in the cloud of about 10^3 photons cm^{-2} s^{-1} (35,36). This is sufficient to produce a stored radical concentration of about 1% in a grain mantle in about $2x10^4$ yrs. A larger concentration of radicals is inhibited by recombination of "hot", diffusing radicals with stored radicals. However, transient heating of grain mantles by cosmic rays to about 30K occurs at a similar timescale (37) and will lead to diffusion and reaction

of these stored radicals. The process can then start over again. Grain-grain collisions with relative velocities in excess of 50 m/s will also produce warming above 30K and can trigger the diffusion and reaction of stored radicals (33).

Extensive laboratory studies have been done on UV photolysis and warm-up of molecular ices containing H_2O, NH_3, CH_3OH, CO, and CH_4 at various concentrations (9,11,34). Besides the original matrix molecules, many simple newly formed molecules (i.e., HCOOH, $HCONH_2$, CO_2, HCO, H_2CO, CH_3OH, HNO) are released upon warm-up. After warm-up above 150K most of the deposited matrix molecules (i.e., H_2O) have evaporated and a refractory residue with an enhanced C abundance is left behind. The composition of some of these residues has been determined by gas chromatography/mass spectrometer analysis (Table 1; 34). Similar molecules are produced by energetic ion bombardment of such ices (38). Typically, these residues consist of small organic molecules with OH, C=O, NH_2 and CH_2 groups and contains 5 to 7 heavy elements of which 2 to 3 are C atoms (smaller molecules generally evaporate below room temperature). Essentially, these molecules are formed by the addition of a few simple building blocks, such as OH, NH_2, and HCO. By adding a few steps to the scheme shown in Fig. 3, plausible reaction networks for their chemical formation can be made (34). In view of the limited number of building blocks, pronounced chemical selectivity will result. In particular, the residues studied are dominated by carboxylic acids, alcohols, and amides, which merely reflects the dominance of saturated hydrides and CO in the initial mixture. Although a different initial mixture may result in a different chemical composition of the residue, we can conclude in general that UV photolysis of icy grain mantles will be chemically specific.

Finally, prolonged exposure to UV photons may eventually lead to the loss of most of the elements other than C. Indeed, there is some laboratory evidence for the formation of unsaturated carbon bonds upon prolonged photolysis. Eventually, such processing may actually lead to an amorphous carbon network, consisting of aromatic units linked by aliphatic chains, similar to that resulting from pyrolysis of terrestrial

kerogen. A rough estimate for the timescale involved for this process in the diffuse interstellar medium is about 1 Myr. Inside dense clouds the UV photon density is too low for this to be of importance. Whether this process is of importance on a galactic scale depends then on the ratio of this conversion timescale to the shock destruction timescale for the organic residue in the diffuse interstellar medium. It is quite conceivable that the latter is relatively long (>10 Myr) and that amorphous carbon - a grain component normally assumed to result from processes around red giants - is also formed in the ISM.

III Interstellar Ice Analog Production

Mid-infrared absorption spectroscopy of dense interstellar clouds generally depends on the presence of embedded or background infrared continuum sources. Fig. 4 illustrates the geometry typical of interstellar absorption objects. Radiation from the source heats the immediately surrounding dust. This hot dust emits an infrared pseudo-blackbody continuum like that shown in the inset close to the protostar in Fig. 4. As this radiation passes through the cloud, molecules along the line-of-sight absorb at their fundamental frequencies resulting in a spectrum which shows absorption features diagnostic of the material (lower inset in Fig. 4). Ice features generally dominate this type of absorption spectra. The key features of interstellar cloud environments shown in Fig. 4 (infrared source, absorbing material, and detection) must be mimicked in laboratory studies of ice analogs.

The spectroscopic study of low temperature solids was developed in the first part of this century. Of particular significance is the matrix isolation approach developed by Pimentel and colleagues (39). The various sample preparation techniques which have evolved over the years, and several theoretical treatments of the interactions in the solid state can be found in various reviews (40-42). The study of interstellar and cometary ice analogs is based on this foundation.

Since the experimental procedures used to study interstellar and

cometary ice analogs have been presented in detail elsewhere (8), the method will only be summarized here. The specific conditions which must be duplicated to create interstellar ice analogs vary widely. Composition, temperature, and exposure to radiation are all parameters that can be duplicated and varied in the laboratory. The general procedure consists of slowly flowing the gas from which the ice is made into a high-vacuum chamber. This gas, which can be a pure substance or a mixture of pure substances, is directed to and condenses on the surface of a substrate cooled by a closed-cycle helium refrigerator or by a cryogen such as liquid helium. A schematic drawing of a typical sample chamber is shown in Fig. 5 and a photograph of the apparatus at Ames is given in Fig. 6. Substrate temperature can generally be maintained anywhere from 10 K to room temperature. The substrate is interchangeable. For infrared studies it is generally a salt (e.g., CsI) window. The substrate is rotatable and is suspended in the center of a sample chamber with gas inlet tubes and several larger ports. The larger openings can be fitted with windows, lamps, ion sources, ovens, pressure gauges, mass spectrometers, phototubes, etc., depending upon the particular ice properties under study. Generally, the substrate is initially positioned to face the gas inlet tube for the preparation of the ice and then rotated to face the other ports as needed. Radiation processing of the sample can be carried out with ultraviolet lamps or ion sources. Photoprocessing of the sample with vacuum ultraviolet radiation is carried out with a microwave powered hydrogen discharge lamp. This has a sharp Lyman α peak at 121.6 nm and a 50 nm broad component centered at roughly 160 nm. Subsequently, the evaporation characteristics of the ice can be studied by measuring spectra during warm-up of the substrate.

The infrared spectrum is measured and plotted as $\log[I_0(\nu)/I(\nu)]$ versus frequency, where $I_0(\nu)$ is the single beam spectrum measured through the substrate before sample deposition and $I(\nu)$ the spectrum measured after. When optical constants (n and k) or integrated absorbance values (A) are to be determined, the infrared transmission spectrum through a sample of known thickness must be measured. Sample thickness

is measured by monitoring the temporal development of the thin film interference pattern of a He-Ne laser beam reflected off or transmitted through the sample during deposition. For a description of the technique and its application to astrophysics as well as a discussion of how to derive n and k values or A values, see ref. (14,18).

IV Infrared Spectroscopy

The infrared spectrum of a compound gives a great deal of information about that compound's structure. This is because molecular transitions which fall in this spectral region occur at the molecule's characteristic vibrational frequencies. While the infrared spectrum is characteristic of the entire molecule, certain groups of atoms give rise to bands at or near the same frequency regardless of the structure of the rest of the molecule. It is the persistence of these characteric group frequencies that make IR spectroscopy such a powerful probe of the composition of interstellar dust and gas. For a thorough description of infrared molecular spectroscopy, the reader is referred to (43), or for a more introductory level to (44). In this section the effects the solid state has on the infrared spectra of molecules will be reviewed in order to analyze the infrared properties of interstellar dust.

A Vibration-rotation spectroscopy

The frequencies of molecular vibrations are determined by the masses of the vibrating atoms, the molecular geometry, and the forces holding the atoms in their equilibrium positions. To a first approximation, the vibrations of a diatomic molecule can be represented as a quantum mechanical harmonic oscillator with the fundamental vibrational frequency, ν, given by

$$\nu = \frac{1}{2\pi}\sqrt{\frac{k}{\mu}} \qquad (1)$$

where k is the chemical bond force constant and μ the reduced mass $[m_1 m_2/(m_1 + m_2)]$, where m_1 and m_2 are the masses of atoms 1 and 2. This formalism can also be used to approximate the stretching frequencies of polyatomic molecules. The combination of the masses of the most cosmically abundant atoms, H, O, C, and N with the kinds of chemical bonds they form restricts most of the fundamental vibrational frequencies for virtually all molecules made up of these atoms to the 4000 to 500 cm^{-1} (2.5-20 μm) region. However, only those modes for which a dipole moment changes during the vibration will give rise to absorption or emission of infrared photons. Thus, the vibrations of all homonuclear diatomic molecules (e.g. O_2, N_2, ...), as well as the centrosymmetric vibrations of symmetric molecules are inaccessible to the infrared spectroscopist.

In general, since certain groups of atoms consistently absorb at or near the same frequency regardless of the rest of the molecule, virtually all molecules containing these groups possess a characteristic vibrational absorption spectrum (45,46). The reason for this, in rather oversimplified language, is that chemical bonds generally fall into three distinct types which are classified as single, double, and triple bonds, depending upon the number of electrons participating in the bond. The term single bond is used to represent a bond in which a total of two electrons occupy the bonding molecular orbital, the double bond has four and the triple bond six. The more bonding electrons, the stronger the force constant and, as implicit in equation (1), the higher the vibrational frequency. Conversely, keeping the type of bond constant but increasing the masses of the vibrating atoms results in a reduction of the fundamental vibrational frequency. This is illustrated in Fig. 7 where the characteristic frequencies of various groups are schematically represented. The stretching vibration of the single bonds C-H, O-H, and N-H all occur near 3000 cm^{-1} whereas the single bonded C-O, C-N or C-C stretch lie in a lower frequency range centered at about 1000 cm^{-1}. Inspection of Fig. 7 also shows that increasing the bond strength from a singly-bonded carbon

through doubly-bonded to triply-bonded carbon implies an increase of the stretching frequency from 1000 cm^{-1} to above 2000 cm^{-1}. As Fig. 7 clearly demonstrates, absorption in each of these specific regions can be used to deduce the type of molecules which are present.

B Solid state effects

Figure 8 shows that there are dramatic differences between the infrared spectrum of a gas phase sample and for the same sample in the solid phase. These differences are due to the following three solid state effects: 1) Rotational Structure Suppression; 2) Line Broadening; and 3) Line Shifting. Each will be discussed in turn.

1) Rotational Structure Suppression

In interstellar clouds, molecules are in both the gaseous and solid phases. In addition to undergoing internal vibrations, molecules in the gas phase can rotate. Since the energies involved in rotational transitions correspond to frequencies of only a few wavenumbers, and selection rules allow rotational transitions to occur simultaneously with vibrational transitions, rotational structure is superimposed on the vibrational transitions. This gives rise to vibration-rotation bands. In the case of symmetric, polyatomic molecules the lines making up a rotation-vibration band produce a recognizable pattern which resembles the rotational level population distribution. The transitions involving an increase in the rotational quantum number J give rise to the so-called R branch, those corresponding to a decrease in J, the P branch, and those with no change in J, the central Q branch. For all heteronuclear diatomics and certain vibrations of linear polyatomics, the Q branch is absent (see top frame Fig. 9). Because molecules are not free to rotate in most ices at 10K, the lines which make up the familiar P and R branches collapse into one broad band which corresponds to the pure vibration. This is illustrated in Fig. 9. In the upper frames the spectrum of gas phase CO is shown at different spectral resolutions. At 2 cm^{-1} resolution, the rotational lines making up

the P and R branches are resolved. At lower resolution, while the individual lines are no longer separable, the rotational profile due to the P and R branches is still recognizable. The spectrum of CO frozen in a molecular ice is shown in the lower frame. Note that, in this case, the vibration occurs at nearly the same frequency as that of gas phase CO i.e.in the null gap or missing Q branch region between 2135 and 2151 cm^{-1}. Figs. 8 and 9 illustrate how rotational line suppression greatly simplify the spectrum of a mixed molecular solid.

2) Line Broadening

In an amorphous, rather than crystalline, solid there is a substantial amount of irregularity in the structure (20). Consequently, each molecule can be situated in a range of different sites. Because of interactions with the environment which are due to a combination of dispersive, steric (geometrical), and dipolar forces, the vibrational frequencies of a molecule in one site can be different from that for the same kind of molecule in another site. Since the spectrum samples a large number of molecules in many different sites, and there is a distribution of sites, a broadened band is produced. Such heterogeneous broadening can range from a few wavenumbers to several hundred wavenumbers, depending on the nature of the interaction and range of sites. For a relatively non-polar molecule such as CO the full width at half maximum spans the range from less than 1 to about 15 wavenumbers. For a strongly hydrogen-bonded molecule such as H_2O , the FWHM can vary from less than one wavenumber in a non-polar solvent to over three hundred wavenumbers in amorphous solid H_2O (12,15).

3) Line Shifting

Shifts from the free gas phase frequency also arise from interactions between the vibrating molecule and the surroundings. Line shifting (and broadening) is caused by the influence neighboring species have on the bond force constant for the particular vibration under consideration. As with line broadening, the stronger the interaction, the

greater the shift. The magnitude of this effect can vary over a large range. In solid CO, for example, the CO stretch occurs at 2138 cm^{-1} , about 5 cm^{-1} lower than the 0-0 transition for gaseous CO while in an $H_2O/CH_3OH/NH_3/CO$ = 20/10/1/1 mixture, it is shifted to 2137 cm^{-1} (19). This rather small shift indicates that there is only a weak interaction between CO and even such strongly polar molecules such as H_2O and NH_3. For molecules which can form weak chemical complexes, or even stronger hydrogen bonds (H-bonds), the shift can be much larger (47). For H_2O, the shift can be greater than 300 cm^{-1} as shown in Fig. 8. Different fundamental vibrations in the same molecule are generally affected differently. For example, as also illustrated in Fig. 8, the fundamental OH stretching frequency in H_2O undergoes a very large shift from 3707 cm^{-1} to about 3300 cm^{-1} and severe line broadening from less than 1 cm^{-1} to over 300 cm^{-1} upon condensation in an H_2O rich ice while the H-O-H bend in the same molecule is far less effected: the shift is only tens of wavenumbers while the width is increased from less than 1 cm^{-1} to about 50 cm^{-1} .

C The IR spectrum of H_2O ice

As an interesting application of these principles and because of its importance in astrophysics, the well known behavior of the OH stretching mode of H_2O, with particular emphasis on the large frequency shift, will be presented in some detail (14,15). When suspended in a non-polar solid (e.g., a CO matrix) H_2O molecules are isolated and do not interact directly with each other and only weakly with the matrix. In this case the OH stretch falls at 3707 cm^{-1}, $\approx$50 cm^{-1} lower than in the gas phase. If the CO is removed, H-bond formation between the H-atoms of one H_2O molecule with the oxygen atom of an adjacent molecule will occur. This attraction of the H-atom by another H_2O molecule causes a substantial reduction of the bond force constant and a correspondingly large shift (nearly 500 cm^{-1}) of the OH stretch to lower frequencies. Of course, an amorphous H_2O structure consists of a wide variety of interaction

geometries and strengths which give rise to an extremely broad band (FWHM ≈ 300 cm^{-1}). This behavior is shown in Fig. 10. The lower trace shows the spectrum for the mixture CO/H_2O = 9/1 in which nearly all of the H_2O molecules are isolated. The absorptions at 3707 and 3673 cm^{-1} are due to H_2O monomers and dimers respectively (48). Upon warm up to 30K, diffusion occurs permitting some of the H_2O molecules to form H-bonds as shown by the increase in absorption due to dimers and higher polymers in the second spectrum. This process continues as the sample is warmed up to even higher temperatures and the CO evaporates. Note also that the absorption coefficient per H_2O molecule undergoes a substantial, anomalous increase as H_2O goes from the monomeric to ice form (49).

Further shifting and broadening can occur if H_2O interacts with a chemical base, such as NH_3 (15). In acid-base terminology, H_2O is neutral and in the presence of a base, at least one of the hydrogen atoms of H_2O will form a complex with this base. This H atom will experience an attractive force greater than it would have when H-bonding with another H_2O molecule, and thus the OH stretching frequency will be even further redshifted than in pure H_2O ice. In the case of H_2O-NH_3 mixtures, the shift is on the order of 800 cm^{-1} and the band is again a few hundred wavenumbers wide. A mixture consisting of comparable amounts of H_2O and NH_3 will be made up of some H_2O molecules H-bonded to other H_2O molecules and some forming acid-complexes with the NH_3. Since absorption due to both forms of H_2O are so broad, the absorption band will be a blend of the two. Because the base-H_2O complex absorption is shifted more than the H-bonded H_2O band, the overall band will resemble that due to amorphous H_2O distorted by a wing on the long wavelength side (15). The absorption strength of the wing with respect to that of the 3250 cm^{-1} component will depend upon how much of each species is present. Note that such a long wavelength wing only implies the presence of a base, not necessarily NH_3.

D Column density determination

The column density of an individual component or type of molecular subgroup in an interstellar ice can only be determined for species in which the integrated absorbance, A, has been measured in an appropriate matrix. The column density of any solid state species can be estimated by

$$N = \frac{\tau_{max}\,\Delta\nu_{1/2}}{A} \qquad (2)$$

where τ_{max} is the optical depth of the band at maximum absorbance, $\Delta\nu_{1/2}$ the FWHM (in cm^{-1}) and A, the integrated absorbance (in cm $molecule^{-1}$). Table 2 lists integrated absorbance values for several astrophysically relevant molecules in the solid state.

This technique has been applied to various absorption bands in protostellar spectra to determine the column density of CO, CN, H_2O and aliphatic carbon (-CH3 and -CH2-) groups on the grains towards these sources (9,19,50-52). The use of this equation will be illustrated by reviewing the calculations of the column density of CO frozen in the icy grain mantles along the line of sight to NGC 7538-IRS 9. The solid CO band in this source shows evidence for two components, a relatively narrow one at 2140 cm^{-1} and a broader one at 2138 cm^{-1}. For the 2140 cm^{-1} component, $\tau_{max} = 2.09$ and $\Delta\nu_{1/2} \approx 5.0$ cm^{-1} has been measured (51). Substituting these values into equation 2 and using $A=10^{-17}$ cm $molecule^{-1}$ appropriate for pure CO (see Table 2), the solid CO column density is calculated to be 10^{18} molecules cm^{-2}. Adding the contribution for the broader 2135 cm^{-1} component, attributed to CO isolated in an H_2O matrix (see §VA), yields a total solid CO column density of 1.8×10^{18} molecules cm^{-2}.

V The Composition of Interstellar Icy Grain Mantles

A IR spectroscopy of protostars

Many objects embedded in or located behind a dense molecular cloud show deep absorption features at 3.08, 4.67, 6.0, 6.85, and 10 μm

(3250, 2140, 1670, and 1460 cm^{-1})[1] in their spectrum (13,22). Fig. 11 shows the composite IR spectrum of one of the best studied objects, W33A. With the exception of the 10 μm (1000 cm^{-1}) band, these features are generally attributed to simple molecules embedded in icy grain mantles along the line of sight. Proposed identifications for these absorption features have recently been reviewed by (13) and only some new developments will be discussed here.

1) The 3.08 μm (3250 cm^{-1}) band

The strong band at 3.08 μm (3250 cm^{-1}) is due to the OH stretching vibration of H_2O ice or mixtures dominated by H_2O. Recent studies have shown that the detailed shape of this band is severely influenced by scattered light (53,54). This is particularly true for the 2.97 μm (3370 cm^{-1}) shoulder on this band, which was previously ascribed to NH_3 (24,55), but which is now thought to result (mainly) from scattering by large ice grains.

The 3.08 μm (3250 cm^{-1}) ice band shows a low frequency wing, whose origin is unclear. It is probably not due to scattering by large particles (56) as evidenced by the polarization study of BN (57). This wing has also been attributed to absorption by H_2O hydrogen-bonded to strong bases such as NH_3 (55,57), but the upper limit on the NH_3 abundance itself is quite small and this base cannot be responsible (13,24). Alternatively, this wing may be caused by overlapping CH stretching absorption features due to organic molecules mixed in with the ice. Indeed, recent higher resolution studies of W33A as well as other protostars have revealed substructure at about 3.5 μm (2860 cm^{-1}) which is well matched in detail with the CH stretching vibration of CH_3OH (Fig. 12; 58). More substructure is present in these spectra, perhaps indicating many blended CH stretching modes in a family of organic compounds. However, this view is not

[1]Throughout the rest of this section band positions will be given in microns as well as wavenumbers, since in the astrophysical literature absorption features are often (confusingly) named after their wavelength position.

universally accepted and further high resolution observations of a larger sample of objects will be very important to resolve this issue.

2) The 4.62 μm (2160 cm^{-1}) band

The 4 to 5 μm (2500-2000 cm^{-1}) region is very characteristic of triple bond and cumulative double bond vibrations. W33A shows a strong band at 4.62 μm (2160 cm^{-1}), which has been assigned to the C≡N stretching mode (51,59). A direct comparison with the laboratory spectrum of a specific candidate molecule has not yet been made. Laboratory UV photolysis studies of simple molecular mixtures containing carbon, nitrogen, and oxygen often show a strong absorption feature at this wavelength which matches the observed interstellar feature very well (Fig. 13; 51). An identification of the carrier as a nitrile or isonitrile seems reasonable (9). It has also been suggested that the laboratory feature, and by inference the interstellar feature, is actually due to the OCN^- ion (60). In salts, this ion shows an absorption feature at about this wavelength, although the exact peak position depends strongly on the cation present. However, no positive evidence for the presence of this anion in the laboratory photolysis studies has been presented. Moreover, the peak frequency of an absorption feature due to an ion will be very sensitive to the local matrix environment (i.e., cation, degree of solvation). Yet the measured laboratory peak frequency does not shift upon warm up, H_2O ice evaporation, and organic residue formation. Clearly, the carrier of this laboratory band cannot be an ion and further laboratory studies are required to identify it. Finally, it has been suggested that the interstellar 4.62 μm (2160 cm^{-1}) band is actually due to the SiH stretching vibration in organic-silicon compounds (61). Such molecular structures may result from UV photolysis of icy molecules containing silicon compounds (e.g., SiH_4). A detailed comparison of these laboratory spectra with the observations could be very interesting.

3) The 4.67 μm (2140 cm^{-1}) band

Many sources show a strong, narrow absorption feature near 4.67

μm (2140 cm^{-1}), which is commonly attributed to solid CO (Fig. 13; 51,52,59,62). Most observed spectra show a narrow (0.01 μm; 4 cm^{-1}) component at ≈4.67 μm (2140 cm^{-1}). Sometimes, a long wavelength wing, probably due to a broad (≈0.02 μm; 9 cm^{-1}), weak, underlying component (≈4.68 μm; 2137 cm^{-1}), is also present. In a few cases an increased width or shifted peak position indicates a different mix (62).

Laboratory studies show that the peak position and shape of the fundamental vibration of CO mixed into cold, molecular ices is a complex function of its interaction with the surrounding matrix (Fig. 14; 19). Among the possible effects are electrostatic dipole-induced dipole interaction as for H_2O/CO complexes (48), the presence of substitutional as well as interstitial sites as in disordered amorphous ices (19), and electron donation by surrounding strong bases (63). The absorption feature due to CO molecules isolated in a matrix dominated by H_2O occurs at about 4.68 μm (2137 cm^{-1}) and has a width of about 0.02 μm (10 cm^{-1}). Pure solid CO absorbs at about 4.675 μm (2139 cm^{-1}) with a width of about 0.005 μm (1 cm^{-1}). Doping of the CO matrix with traces of other species leads to a broadening but little shift of this line. Since the observed 3.08 μm (3250 cm^{-1}) ice band attest to the presence of H_2O dominated ice mantles, it is tempting to attribute the observed, relatively broad, underlying CO component to CO in H_2O dominated grain mantles, while the narrow CO component may be due to more pure CO ices containing little H_2O. Indeed, a reasonable fit to the narrow interstellar component can be obtained with pure CO (62). Thus, these CO observations do reveal, for the first time, the presence of at least two distinct grain mantle components along the same line of sight in interstellar clouds.

4) <u>The 6.0 and 6.85 μm (1670 and 1460 cm^{-1}) bands</u>

The 5-8 μm (2000-1250 cm^{-1}) region is characteristic for CH, NH, and OH bending and deformation modes and the strong carbonyl (C=O) stretching mode. Two absorption features, at 6.0 and 6.85 μm (1670 and 1460 cm^{-1}), have been detected in this wavelength region in protostellar objects. These have been attributed to the OH bending mode in H_2O and the

CH deformation mode in CH_3OH, respectively (50). Some low resolution ($\lambda/\Delta\lambda \approx 50$), interstellar spectra have shown evidence for spectral structure in this wavelength region which has been interpreted in terms of carbonyl-bearing molecules such as H_2CO (13). Recent moderate resolution ($\lambda/\Delta\lambda \approx 150$) spectra obtained with the KAO are in good agreement with previous lower resolution spectra (Fig. 15). The features in the spectrum of W33A are indeed fitted very well by laboratory spectra of H_2O and CH_3OH (Fig. 15). The latter identification is, however, not unequivocally accepted (see below). Carbonyl-bearing molecules (eg., H_2CO) show a strong C=O stretching vibration at about 5.8 μm (1720 cm^{-1}). The smoothness of the 6.0 μm (1670 cm^{-1}) feature in W33A implies an upper limit of about 0.2 % on the abundance of C=O groups with respect to H_2O.

The spectrum of Mon R2-IRS 2 is strikingly different from that of W33A. Rather than the presence of carbonyl groups as previously suggested (50), these higher resolution observations show that this is due to the presence of strong PAH emission features at 6.2, 7.7, and probably 5.2 μm (1610, 1300, and 1920 cm^{-1}). Note that the 7.7 μm feature in this source is particularly well resolved in the well known components at about 7.5 and 7.8 μm (1330 and 1280 cm^{-1}; 64). The ArII line at 6.99 μm is also obvious at this resolution. These emission features probably arise in the nearby compact HII region associated with Mon R2-IRS 1. Although a narrow 6.0 μm (1670 cm^{-1}) absorption band similar to that in W33A seems to be present in this source, there is little evidence for a 6.85 μm (1460 cm^{-1}) absorption band.

Perhaps not surprising, the Leiden group has recently suggested that, like their assignment of the 4.62 μm (2160 cm^{-1}) band, the 6.85 μm (1460 cm^{-1}) band is also due to an ion produced by UV photolysis (i.e., $R\text{-}NH_3^+$ or NH_4^+; 34,65). Laboratory UV photolysis studies on NH_3/O_2 mixtures demonstrate that a simple nitrogen and/or oxygen containing compound produces an absorption feature around 6.7 μm (1490 cm^{-1}). A similar band appears upon UV photolysis of a $H_2O/NH_3/CO/O_2$ (10/1/1/1) mixture, which by inference is then attributed to the same

compound. This band shows considerable shift upon warm up, consistent with ion-solvation (or annealing) effects. A good fit to the interstellar band can be obtained with a sample warmed up to 180 K (65). However, similar processing of other equally relevant interstellar mixtures does not provide such a good agreement (9,34). The temperature sensitivity is also difficult to reconcile with the similarity in the 6.85 μm (1460 cm^{-1}) profile observed in a variety of sources. Indeed, the shape of this band in W33A, NGC 7538-IRS 9, W3 IRS 5, and AFGL 2136 is very similar despite the large difference in optical depth (13). In contrast, the invariance of the shape is readily understood assuming CH_3OH absorption. This and the detection of the 3.5 μm (2860 cm^{-1}) absorption (see Fig. 12) makes CH_3OH the preferred interpretation in the authors' opinion.

B Grain mantle abundances

Table 3 summarizes typical abundances for several interesting molecules in interstellar icy grain mantles relative to H_2O. This molecule always has the largest column density along a line of sight. However, as discussed above, the solid CO data implies the existence of at least two, distinctly different grain mantle components along many lines of sight. Typical estimates for the solid CO abundance in these two components are listed separately in Table 3. Although many questions remain, a suggestive comparison can be made between observed and calculated abundances (Table 3). For example, several of the molecules predicted to be present have been observed with approximately the right abundance. The detection of grain mantles dominated by non-polar molecules, rather than H_2O, is also in good agreement with theoretical predictions. The detection of oxygen-rich interstellar grain mantles (ie., CO_2, O_3) probably has to await space-borne IR spectrometers on ISO and SIRTF.

There is some controversy on the abundance of CH_3OH. The abundance inferred from the 3.5 μm (2860 cm^{-1}) band is much lower than that obtained from the 6.85 μm (1460 cm^{-1}) band and may imply that the latter is largely due to molecules other than CH_3OH (58). However, part of

this discrepancy may actually reflect the uncertainty in the underlying continuum of the 3.5 μm (2860 cm^{-1}) band due to the low frequency wing of the 3.08 μm (3250 cm^{-1}) ice band and the blending of overlapping CH stretching bands (see § VA 1). Moreover, in a circumstellar disk/scattering nebula geometry, the ratio of absorption features in different parts of the spectrum can be distincly different from their intrinsic value (54). Essentially, near-infrared photons preferentially result from scattering into the beam of photons "escaping" through the poles, while mid-infrared photons are directly emitted into the beam by the stellar (or dust) photosphere. As a result, the near-infrared wavelength photons will encounter less absorption than expected from the strength of mid-infrared absorption features. Since most protostars seem to be embedded in near-infrared reflection nebulae and the shape of the 3.08 μm (3250 cm^{-1}) feature is often affected by scattering, this is probably a common effect. Indeed, the ratio of the 3.08 μm to the 6.0 μm band, both generally attributed to H_2O, is observed to vary by a factor 3 from source to source (13). In the analysis of grain mantle abundances (Table 3) we have therefore relied on column densities derived from the mid-infrared absorption features.

C Organic Refractory Grain Mantles

It is of some interest to consider the observational constraints on the abundance of the organic refractory grain mantles resulting from the irradiation of these icy mixtures. Laboratory studies suggest that about 1% by mass of the original ice mixture is converted into such a residue in one irradiation-warm up cycle (34). Since over the lifetime of a cloud many such cycles would occur, as much as 30% of all the carbon is then expected to be locked up in organic refractory grain mantles (20). This seems excessive, since the IR spectra of protostars are dominated by simple ices (see § VA), containing typically only 5% of the O and perhaps an equal amount of C, rather than by organic residues. In particular, presently, only the 4.62 μm band is generally attributed to UV photolyzed

grain mantles. All other observed absorption features are reasonably well accounted for by species produced by accretion and surface reactions. Absorption features due to organic residues in the 3 μm region of interstellar spectra may be "hidden" to some extent by the strong 3.08 μm (3250 cm^{-1}) ice band. However, the 5-8 μm laboratory spectra of such residues (9,34) also show various strong absorption bands, which are not obvious in interstellar spectra. It seems that organic residues are not as abundant as these laboratory experiments suggest and may contain perhaps upto 5% of the elemental C or O. Further high quality spectroscopic studies of protostars are of utmost importance to detect the weak bands and substructure expected to be associated with these organic residues.

VI Summary

Infrared absorption and emission spectroscopy of infrared continuum sources embedded in or behind dense molecular clouds provide a powerful means of probing the composition of cosmic dust and the physical and chemical nature of the environments in which it is found. Comparison of laboratory absorption spectra of various materials with astronomical spectra indicates that the bulk of the absorption features associated with dark clouds are attributable to mixed molecular ices. H_2O dominates the composition of interstellar ices. CH_3OH may also be an important ice component. However, analysis of the various profiles and positions of the interstellar solid CO feature near 2138 cm^{-1} (4.67 μm) suggest a more complex picture. Molecular clouds seem to contain at least two distinct types of ice; one characterized by polar, hydrogen-bonding molecules like H_2O, and the other characterized by non-polar, or only slightly polar molecules, possibly CO itself. Such an interpretation would have been impossible without a great deal of prior laboratory work. Although many questions remain, a favorable - but non-unique - comparison can be made with the theoretical models which incorporate gas and grain-surface reactions. Finally, comparisons between the

interstellar and laboratory spectra suggest that interstellar ices along some lines-of-sight also contain species which cannot be formed by simple gas-gas or gas-grain interactions. Probably these results from irradiation of the icy mixtures.

Acknowledgements: Laboratory studies of interstellar ices at NASA Ames Research Center is supported under RTOP 199-52-12-04.

References:

1) Trumpler, R. J. (1930). *P.A.S.P.*, **42**, 267.
2) Huffman, D. R. (1977). *Adv. Phys.*, **26**, 129, and references therein.
3) Moore, M. H., Donn, B., Khanna, R., and A'Hearn, M. F. (1983), *Icarus,* **54**, 388.
4) Strazzulla, G., Pirronello, V., and Foti, G. (1983), *Astr. Ap.,* **123**, 93.
5) Johnson, R. E., Lanzerotti, L. J., Brown, W. L., Augustyniak, W. M., and Mussil, C. (1983), *Astr. Ap.,* **123**, 343.
6) Lanzerotti, L. J., Brown, W. L., and Johnson, R. E. (1984), in *Ices in the Solar System*, eds. J. Klinger, D. Benest, A. Dollfus, and R. Smoluchowski, (Reidel, Dordrecht), p.317.
7) Johnson, R. E., Cooper, J. F., and Lanzerotti, L. J. (1986), Proc. 20th ESLAB Sym. on Exploration of Halley's Comet, ESA SP-250, Vol. II, 269.
8) Hagen, W., Allamandola, L. J., and Greenberg, J. M. (1979), *Astr. Space Sci.,* **65**, 215.
9) d'Hendecourt, L. B., Allamandola, L. J., Grim, R. J. A., and Greenberg, J. M., (1986), *Astr. Ap.,* **158**, 119.
10) Grim, R. J. A., and Greenberg, J. M. (1987), *Astr. Ap.,* **181**, 155.
11) Allamandola, L. J., Sandford, S. A., and Valero, G. J. (1988), *Icarus*, **76**, 225.
12) Allamandola, L. J. (1984), in *Galactic and Extragalactic Infrared Spectroscopy*, eds., M. Kessler and P. Phillips, (Reidel, Dordrecht), p. 5.

13) Tielens, A. G. G. M., and Allamandola, L. J. (1987), *Physical Processes in Interstellar Clouds,* eds. G. E. Morfill and M. Scholer, (Reidel, Dordrecht), p. 333.
14) Hagen, W., Tielens, A. G. G. M., and Greenberg, J. M. (1981), *Chem. Phys.*, **56**, 367.
15) Hagen, W., Tielens, A. G. G. M., and Greenberg, J. M. (1983), *Astr. Astr. Suppl. Ser.*, **51**, 389.
16) Kitta, K., and Kratschmer, W., 1983, *Astr. Ap.*, **122**, 105.
17) Leger, A., Gauthier, S., Defourneau, D., and Rouan, D. (1983), *Astr. Ap.*, **117**, 164.
18) d'Hendecourt, L. B., and Allamandola, L. J. (1986), *Astr. Ap. Suppl. Ser.*, **64**, 453.
19) Sandford, S. A., Allamandola, L. J., Tielens, A. G. G. M., and Valero, G. J. (1988), *Ap. J.,* **329**, 498.
20) Tielens, A.G.G.M., and Allamandola, L.J., 1987, in *Interstellar Processes*, eds. D. Hollenbach and H. Thronson, (Reidel, Dordrecht), p.397.
21) Allamandola, L.J., and Sandford, S.A., in *Dust in the Universe*, eds. M.E. Bailey and D.A. Williams, (Cambridge Univ. Press, Cambridge), p.229.
22) Tielens, A.G.G.M., 1989, in *Interstellar Dust,* eds. L.J. Allamandola and A.G.G.M. Tielens, (Reidel, Dordrecht), p.239.
23) Irvine, W. M., Goldsmith, P.F., and, Hjalmarson, Å, 1987, in *Interstellar Processes*, eds. D. Hollenbach and H. Thronson, (Reidel, Dordrecht), p.561.
24) Tielens, A. G. G. M., and Hagen, W. (1982), *Astr. Ap.*, **114**, 245.
25) Tielens, A.G.G.M., 1983, *Astr. Ap.*, **119**, 177.
26) d'Hendecourt, L. B., Allamandola, L. J., and Greenberg, J. M. (1985), *Astr. Ap.*, **152**, 130.
27) Brown, P.D., Charnley, S.B., and Millar, T.J., 1988, *M.N.R.A.S.*, **231**, 409.
28) Zhao, N., 1989, private communication.
29) Grim, R. J. A., and d'Hendecourt, L. B. 1986, *Astr. Ap.*, **167**, 161.

30) Tielens, A.G.G.M., and Hagen, W., 1982, unpublished.
31) Dalgarno, A., and Lepp, S. 1985, *Ap.J. Letters*, **287**, L47.
32) Greenberg, J. M., 1979, in *Stars and Stellar Systems*, ed. B. Westerlund, (Dordrecht: Reidel), p. 173.
33) d'Hendecourt, L. B., Allamandola, L. J., Baas, F., and Greenberg, J. M. 1982, *Astr. Ap.*, **109**, L12.
34) Schutte, W. 1988, *Ph. D. Thesis*, RijksUniversiteit Leiden.
35) Prasad, S. S., and Tarafdar, S. P. 1983, *Ap. J.*, **267**, 603.
36) Sternberg, A., Dalgarno, A., and Lepp, S., *Ap. J.*, **320**, 676.
37) Léger, A., Jura, M., and Omont, A. 1985, *Astr. Ap.*, **144**, 147.
38) Rössler, K., 1986, *Rad. Eff.*, **99**, 21, and references therein.
39) Pimentel, G. C. (1960), in *The Formation and Trapping of Free Radicals*, eds., A.M. Bass and H.P. Broida, (Academic Press, New York), p.69.
40) Meyer, B., 1971, *Low Temperature Spectroscopy*, (Elsevier, Amsterdam).
41) Hallam, H.E., 1973, *Vibrational Spectroscopy of Trapped Species*, (Wiley &Sons, New York).
42) Ozin, G. and Moscovitz, H., 1976, *Cryochemistry*, (Wiley & Sons, New York).
43) Herzberg, G.H., 1968, *Infrared and Raman Spectra of Polyatomic Molecules*, (van Nostrand Company, Princeton).
44) Barrow, J.M., 1962, *Introduction to Molecular Spectroscopy*, (McGraw-Hill, New York).
45) Silverstein, R. M., and Bassler, G. C. (1967), *Spectrometric Identification of Organic Compounds, Chapter 3: Infrared Spectrometry*, (Wiley & Sons, New York), p.64.
46) Bellamy, L. J. (1958), *The Infrared Spectra of Complex Organic Molecules*, (Wiley & sons, New York).
47) Pimentel, G.C., and McClellan, 1960, *The Hydrogen Bond*, (Freeman, San Fransisco).
48) Hagen, W, and Tielens, A.G.G.M., 1981, *J. Chem. Phys.*, **75**, 4198.
49) van Thiel, M., Becker, E. D., and Pimentel, G. C. (1957), *J. Chem. Phys.*,

27, 486.
50) Tielens, A. G. G. M., Allamandola, L. J., Bregman, J., Goebel, J., d'Hendecourt, L. B., and Witteborn, F. C 1984, *Ap. J.*, **287**, 697.
51) Lacy, J. H., Baas, F., Allamandola, L. J., Persson, S. E., McGregor, P. J., Lonsdale, C. J., Geballe, T. R., and van der Bult, C. E. P. (1984), *Ap. J.*, **276**, 533.
52) Geballe, T. R. (1986), *Astr. Ap.*, **162**, 248.
53) Knacke, R. F., and McCorkle, S. M. 1987, *Astron. J.*, **94**, 972.
54) Pendleton, Y., Tielens, A. G. G. M., and Werner, M. W. 1990, *Ap. J.*, **349**, in press.
55) Knacke, R. F., McCorkle, S. M., Puetter, R. C., Erickson, E. F., and Kratschmer, W. 1982, *Ap. J.*, **260**, 141.
56) Merrill, K. M., Russell, R. W., and Soifer, B. T. 1976, *Ap. J.*, **207**, 763.
57) Hagen, W., Tielens, A. G. G. M., and Greenberg, J. M. 1983, Astr. Ap., **117**, 132.
58) Grim, R., Baas, F., Schutte, W., Greenberg, M., and Geballe, T., *Astr. Ap.*, submitted.
59) Larson, H. P., Davis, D. S., Black, J. H., and Fink, U. 1985, *Ap. J.*, **299**, 873.
60) Grim, R. J. A., and Greenberg, J. M. 1987, *Ap. J. Letters*, **321**, L91.
61) Nuth, J. A., and Moore, M. H. 1988, *Ap. J. Letters*, **329**, L113.
62) Tielens, A. G. G. M., Tokunaga, A., Geballe, T. R., and Baas, F. 1989, in preparation.
63) Hollim, P., and Pritchard, J. 1980, in *Vibrational Spectroscopy for Adsorbed Species*, eds. A. T. Bell and M. L. Hair, (New York: Acad. Press), p. 51.
64) Bregman, J. D., 1989, in *Interstellar Dust*, eds. L. J. Allamandola and A. G. G. M. Tielens, (Dordrecht: Reidel), p.109.
65) Grim, R. J. A. 1988, *Ph. D. Thesis*, RijksUniversiteit Leiden.
66) Jiang, G.J., Person, W.B., and Brown, K.G., 1975, *J. Chem. Phys.*, **62**, 1201.
67) Sandford, S.A., and Allamandola, L.J., *Ap. J.*, submitted, and references therein.

Figure Legends

Fig. 1: Representation of the types of core-mantle grains expected in molecular clouds.

Fig. 2: A comparison of the calculated gas phase and solid state composition of a molecular cloud. When atomic H dominates over heavy species in the gas phase, accreting species will be hydrogenated. Otherwise grain mantles will reflect the gas phase more directly. Note that large deuterium enrichments are expected to be a characteristic of grain mantles as a result of the high atomic D/H ratio in the gas phase (adapted from ref. 24,25).

Fig. 3: Possible reaction pathways involving CO in an interstellar grain mantle illustrating how the intermediates H, OH, CH_3, and NH_2 can add to CO and produce a very rich chemical mixture.

Fig. 4: Schematic of how one obtains absorption spectra of interstellar ices.

Fig. 5: Schematic representation of the interstellar and cometary ice analog sample chamber at NASA Ames Research Center.

Fig. 6: Photograph of an Ice Analog sample chamber at NASA Ames Research Center. The base is approximately 10 cm on a side and the cold window is about 2 cm in diameter.

Fig. 7: Vibrational frequency ranges of various molecular groups.

Fig. 8: A comparison between the infrared of the mixture H_2O : CO : CH_3OH : NH_3 (6:3:3:2) in the gas phase at room temperature and as an amorphous solid at 10 K. Both spectra taken at 1 cm^{-1} resolution.

Fig. 9: The spectrum of CO in the gas phase and in a mixed molecular ice. The spectral resolution is indicated by RES.

Fig. 10: The evolution of the infrared absorbance spectrum of an H_2O : CO (1:9) mixture as the sample is warmed up from 10 K. All spectra are plotted on the same absorbance scale. From bottom to top: a) immediately after deposition at 10 K; b) after warm up to 30 K without CO evaporation; c,d) after CO evaporation above 30 K (taken from 48).

Fig. 11: The infrared spectrum of the protostar W33A. Identifications for the observed absorption features in terms of simple "icy" molecules are indicated on the top (see ref. 13). Some of these are, however, not unequivocally accepted. The deep 10 μm band is generally attributed to refractory silicates. See text for details.

Fig. 12: A weak feature at about 3.5 μm has been detected in the spectrum of W33A (dots; 58). It seems to be present in the spectra of other sources as well. A good match to the shape of this feature is obtained with solid CH_3OH (solid line).

Fig. 13: The laboratory spectrum in the 2100-2200 cm^{-1} region of an NH_3/CO ice which has been photolyzed and warmed up to 150 K compared to the spectrum of W33 A. Figure adapted from ref. (51).

Fig. 14: The CO stretching mode for CO suspended in various molecular mixtures at 10 K. Adapted from ref. (19).

Fig. 15: Recent 5-8 μm spectra of two protostars. W33A shows absorption features at 6.0 and 6.85 μm (1670 and 1460 cm^{-1}) which are particularly well matched by the laboratory spectra of

H_2O and CH_3OH, respectively. Although a weak 6.0 μm absorption feature may be present, the spectrum of Mon R2-irs 2 is dominated by the well known 6.2 and 7.7 μm emission features due to PAH molecules and the ArII and Pfa emission lines. Recognition of these emission components in previous studies was hampered by insufficient resolution.

TABLE 1: THE COMPOSITION OF AN ORGANIC RESIDUE[1]

Species	Formula	Abundance
Glycolic acid	$HOCH_2COOH$	0.38
Hydroxyacetamide	$HOCH_2CONH_2$	0.13
Oxamic acid	$H_2NCOCOOH$	0.05
Glycerol	$HOCH_2CHOHCH_2OH$	0.06
Oxamide	$H_2NCOCONH_2$	0.15
Glyceric acid	$HOCH_2CHOHCOOH$	0.07
Glyceramide	$HOCH_2CHOHCONH_2$	0.16

[1] Initial mixture $H_2O/CO/CH_4/NH_3$=10/3/3/1

Table 2: Infrared Integrated Absorbance values for molecules of astrophysical interest in the solid state.

molecule	mode	frequency [cm^{-1}]	λ [μm]	A [cm/molecule]
H_2O[a]	OH stretch	3257	3.07	2 (-16)
	OH bend	1670	6.00	8 (-18)
	Libration	750	13.3	3 (-17)
CO	stretch in CO[b]	2139	4.675	1 (-17)
	stretch in H_2O[c]	2137	4.680	2 (-17)
CO_2[d]	stretch in CO_2	2343	4.268	8 (-17)
	stretch in H_2O	2342	4.270	2 (-16)
	bend in CO_2	660,665	15.2, 15.3	1 (-17)
	bend in H_2O	653	15.3	4 (-17)
CH_4[e]	CH stretch	3010	3.322	6 (-18)
	CH deformation	1300	7.692	6 (-18)
NH_3[e]	NH stretch	3375	2.963	1 (-17)
	umbrella	1070	9.346	2 (-17)
CH_3OH[e]	OH stretch	3250	3.077	1 (-16)
	CH stretch	2982	3.354	2 (-17)
	CH stretch	2828	3.536	8 (-18)
	CH & OH deform.	"1455"	"6.87"	1 (-17)
	CO stretch	1026	9.747	2 (-17)
Hexane[e,f]	CH stretch[g]	2955	3.384	1 (-17)
		2870	3.484	2 (-18)
	CH stretch[h]	2921	3.424	5 (-18)
		2858	3.499	1 (-18)
	CH deform.[i]	"1465"	"6.83"	1 (-18)

	CH_3 deform.[g]	1370	7.299	2 (-19)
CH_3CN[e]	CN stretch	2270	4.405	2 (-18)
Ethylacetate[e,j]	C=O stretch	1738	5.754	4 (-17)
	CH stretch[g]	2986	3.349	2 (-18)
	CH_2 deform.[h]	1450	6.897	8 (-18)
	CH_3 deform.[g]	1375	7.273	4 (-18)

notes: a) ref. (14,15); b) ref. (66); c) ref. (19); d) ref. (67), Absorption strength in CO similar, but peak positions slightly shifted; e) ref. (18); f) $CH_3(CH_2)_4CH_3$; g) per $-CH_3$ group; h) per $-CH_2-$ group; i) per $-CH_3$ and $-CH_2-$ group; j) $CH_3(CO)OCH_2CH_3$.

TABLE 3: COMPOSITION OF INTERSTELLAR ICY GRAIN MANTLES

	Absorption features		Abundance[1]	
Species	λ [μm]	ν [cm^{-1}]	Observed	Calculated[2]
H_2O	3.08	3250	—	—
	6.00	1650	100	100
CO[3]	4.68	2135	0-5	0.4
	4.67	2140	0-25	—
CH_3OH	3.5	2830	7[4]	—
	6.85	1460	50	(40)[5]
XCN	4.61	2167	(4)[6]	—
OCS	4.90	2040	(0.05)[7]	0.4
NH_3	2.95	3375	< 5	1
	6.10	1625	—	—
H_2S	3.94	2540	0.3	0.03
CH_4	7.70	1300	< 1	0.007
H_2CO	3.53	2835	< 0.2	(0)[5]
	5.80	1720	—	—
CO_2	4.28	2337	—[8]	9

[1]Abundances of molecules in grain mantles relative to H_2O=100.
[2]Calculated abundances for a reducing atmosphere (n_o = 10^4 cm^{-3}; 24)
[3]The 4.68 and 4.67 μm bands refer to the two independent CO components observed. Both abundance estimates are relative to the total H_2O (ice) column density along the line of sight.
[4]The observed abundance of CH_3OH is controversial (see text).
[5]Assuming all H_2CO converted into CH_3OH by grain surface reactions.
[6]Thought to result from UV photolysis. Abundance estimated from laboratory studies.
[7]Assuming absorption is due to OCS.
[8]Presently unobservable due to telluric CO_2.

GRAIN MANTLE GROWTH AND EVOLUTION

GRAIN SURFACE REACTIONS PRODUCE SIMPLE MOLECULES

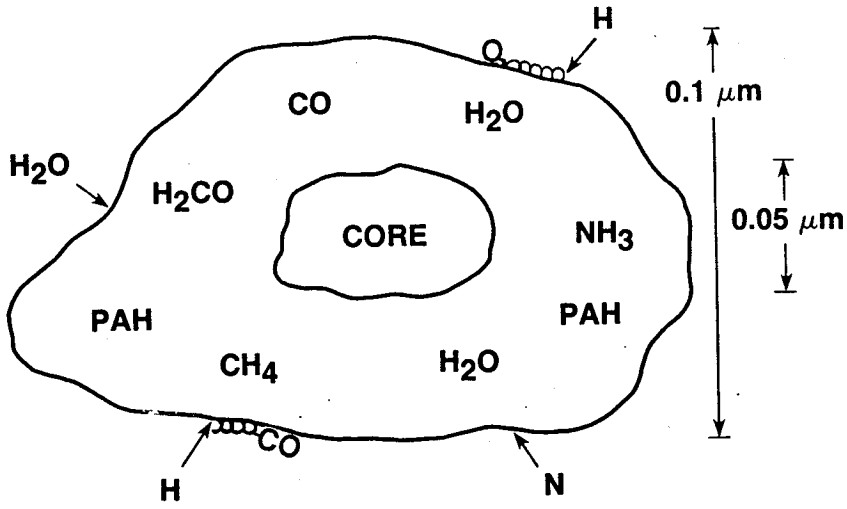

UV IRRADIATION PRODUCES COMPLEX MOLECULES

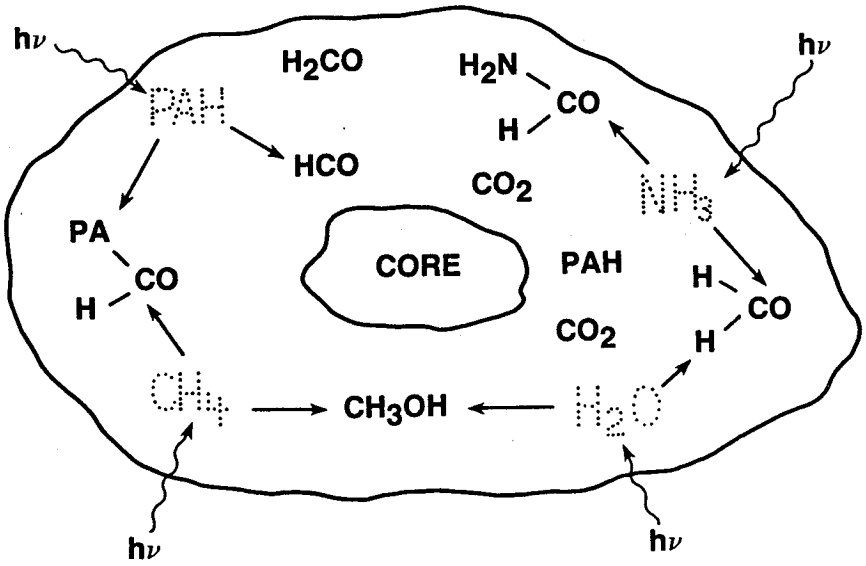

WITHOUT SOME FORM OF ENERGETIC PROCESSING, MANTLES WILL BE MADE UP PRIMARILY OF SIMPLE MOLECULES

Fig 2

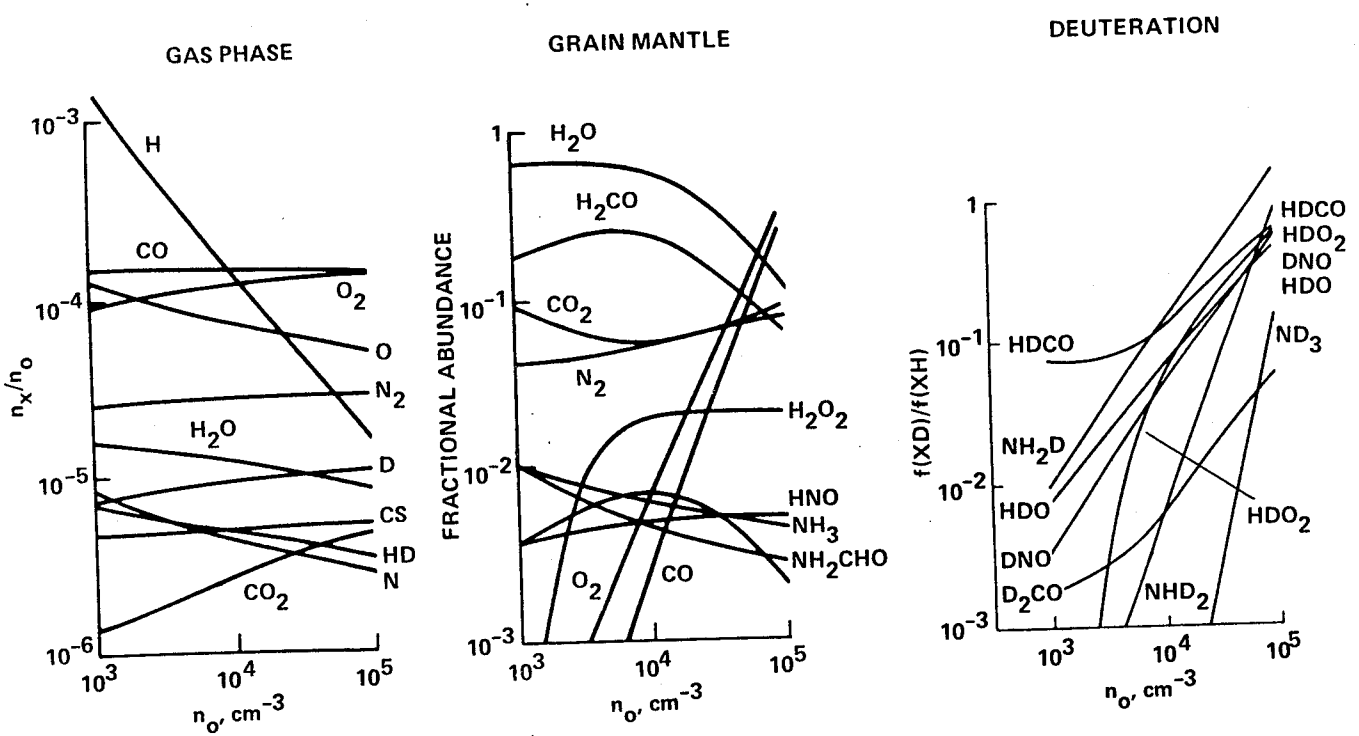
GAS PHASE
GRAIN MANTLE
DEUTERATION
10^{-3}
10^{-4}
10^{-5}
10^{-6}
n_x/n_o
H
CO
O_2
O
N_2
H_2O
D
CS
HD
N
CO_2
10^3
10^4
10^5
n_o, cm^{-3}
1
10^{-1}
10^{-2}
10^{-3}
FRACTIONAL ABUNDANCE
H_2O
H_2CO
CO_2
N_2
H_2O_2
HNO
NH_3
NH_2CHO
O_2
CO
f(XD)/f(XH)
HDCO
HDO_2
DNO
HDO
ND_3
NH_2D
D_2CO
NHD_2

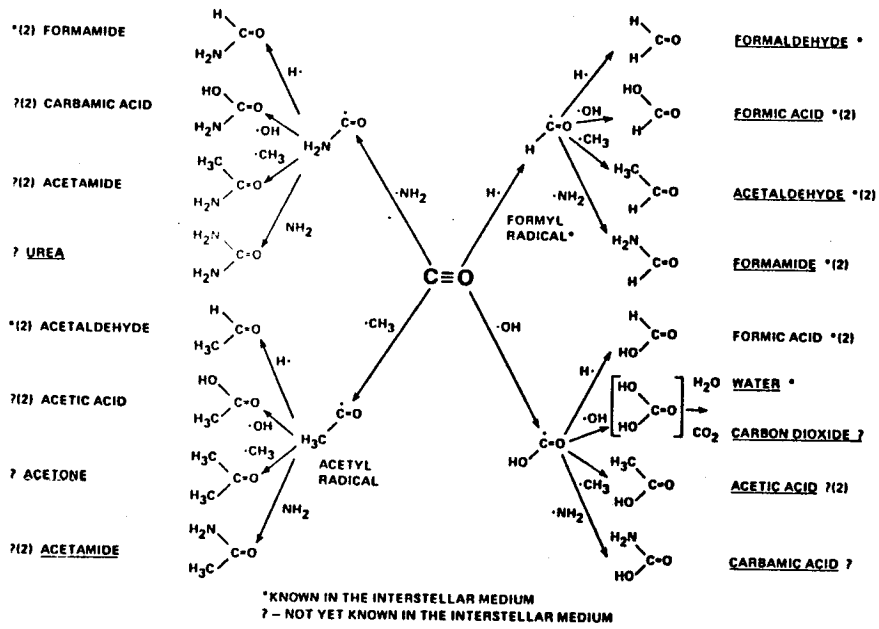

*KNOWN IN THE INTERSTELLAR MEDIUM
? – NOT YET KNOWN IN THE INTERSTELLAR MEDIUM

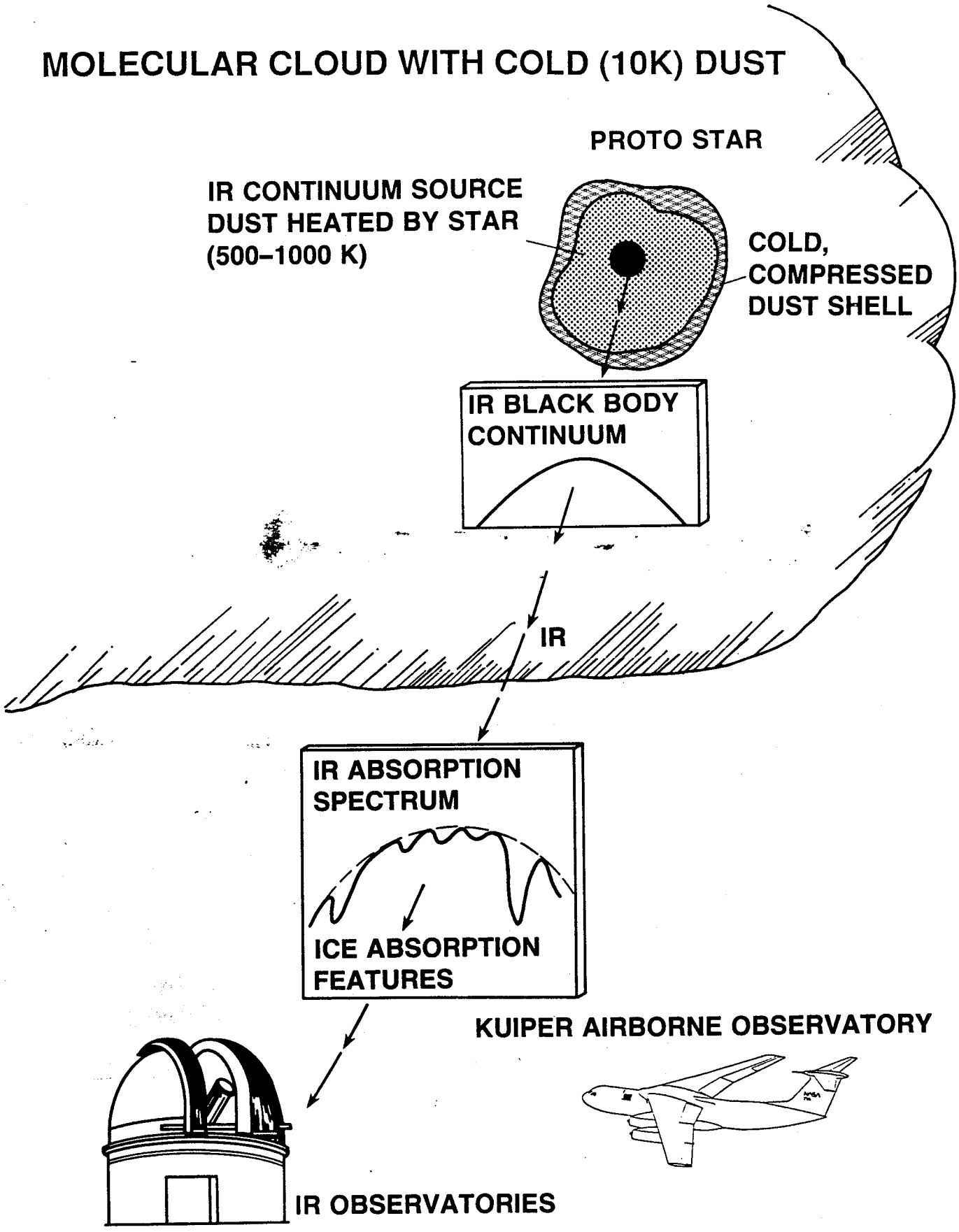
MOLECULAR CLOUD WITH COLD (10K) DUST
PROTO STAR
IR CONTINUUM SOURCE
DUST HEATED BY STAR
(500–1000 K)
COLD,
COMPRESSED
DUST SHELL
IR BLACK BODY
CONTINUUM
IR
IR ABSORPTION
SPECTRUM
ICE ABSORPTION
FEATURES
KUIPER AIRBORNE OBSERVATORY
IR OBSERVATORIES

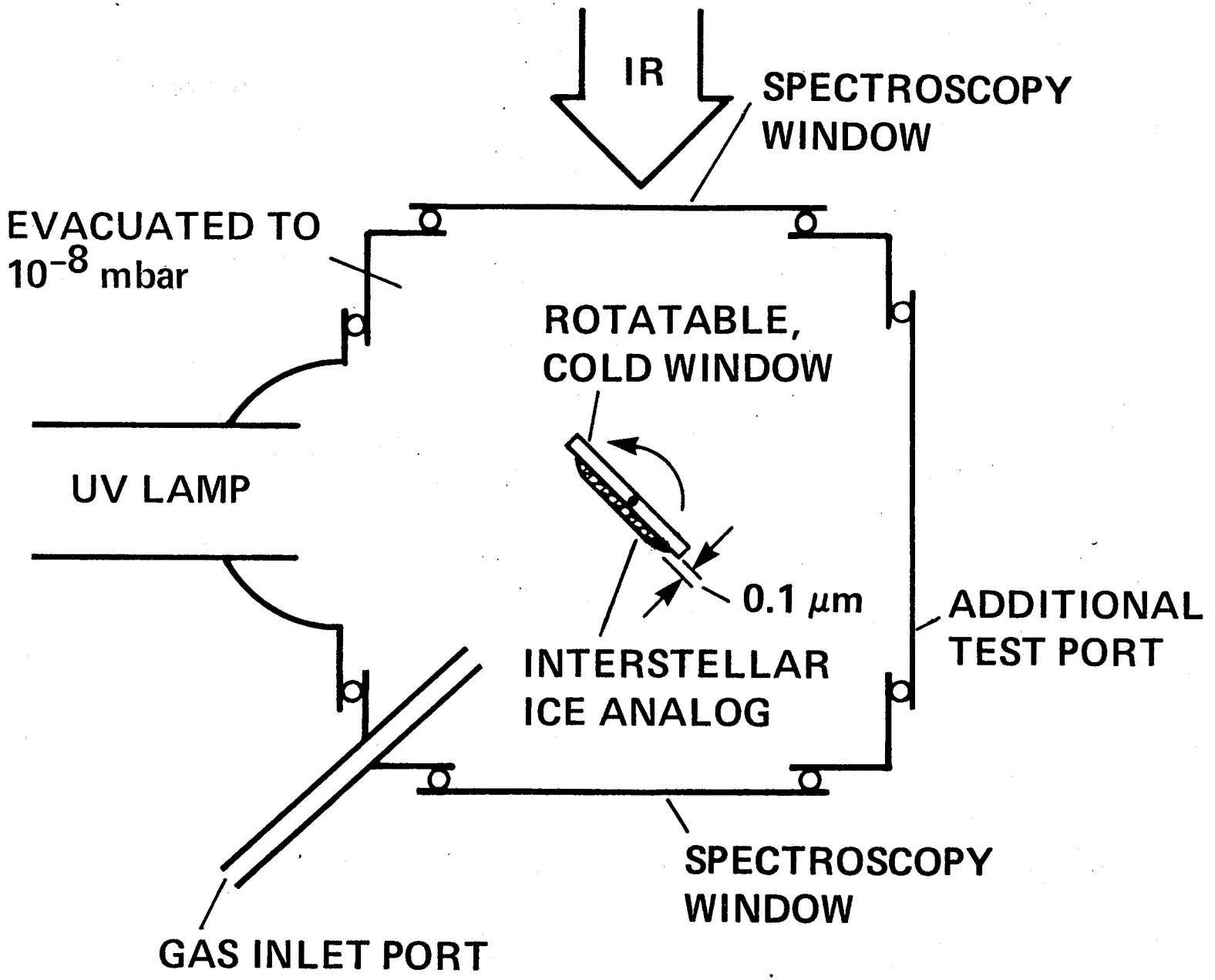

Schematic of sample chamber, top view.

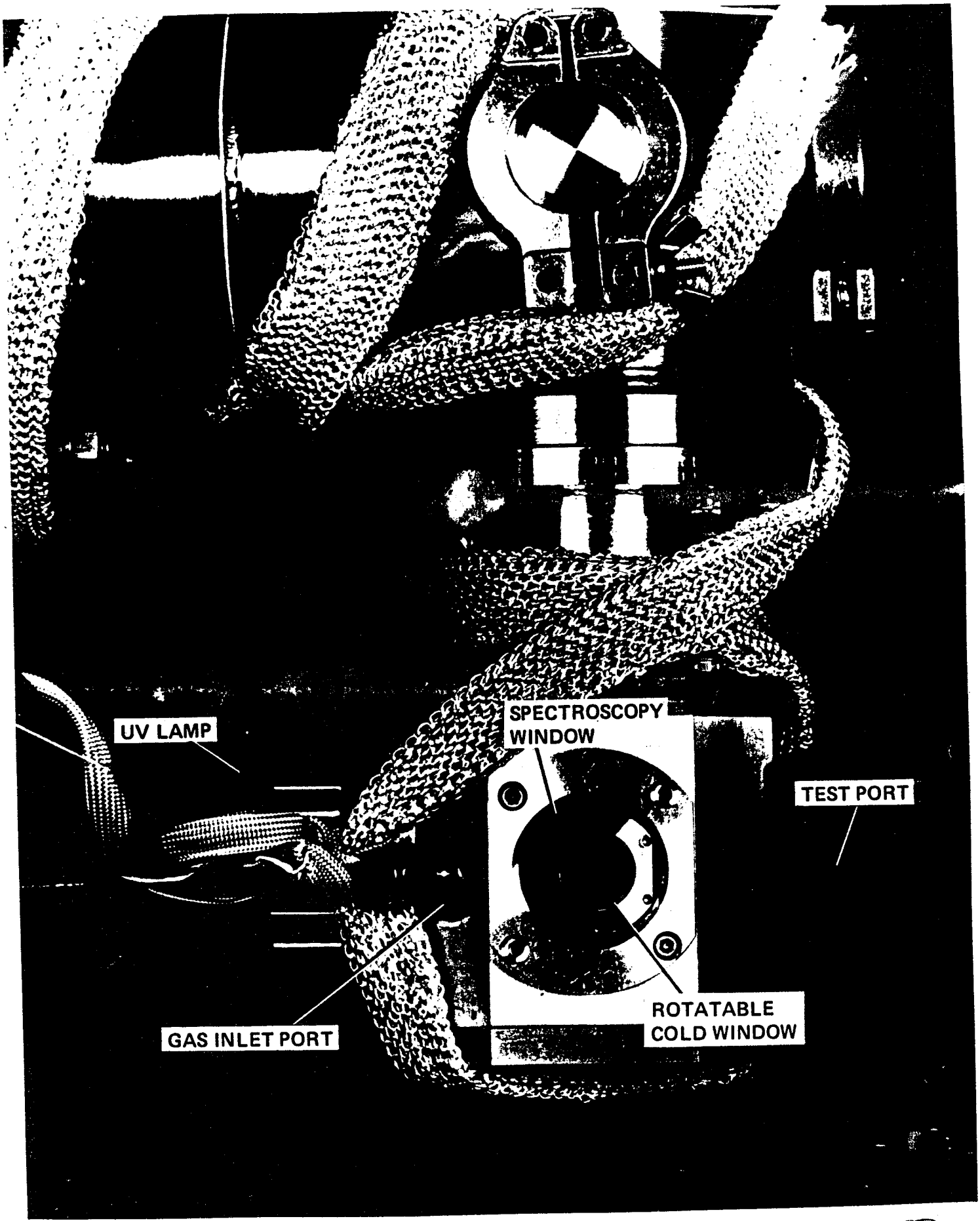
UV LAMP
SPECTROSCOPY WINDOW
TEST PORT
GAS INLET PORT
ROTATABLE COLD WINDOW

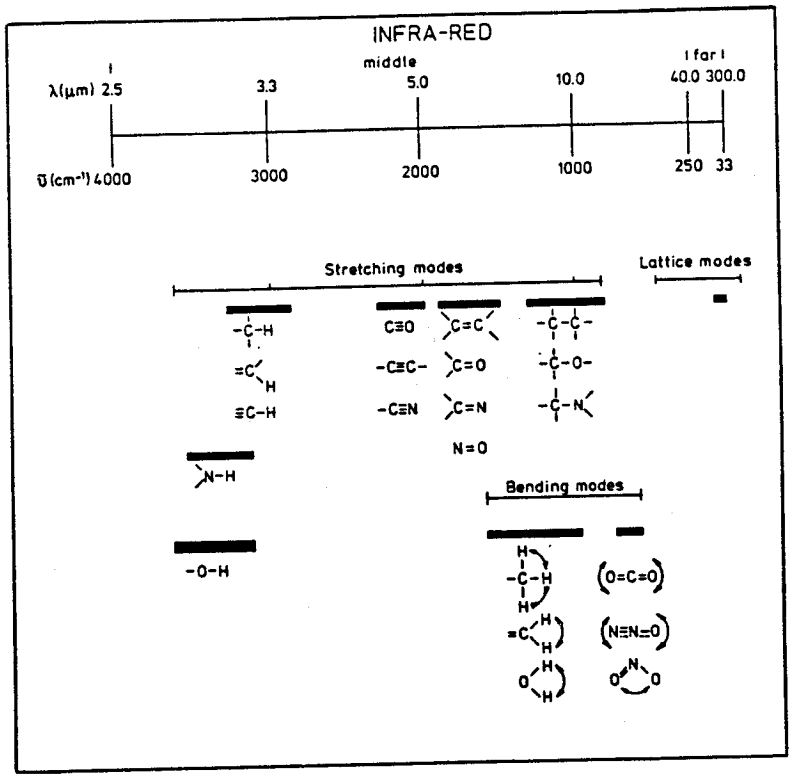
INFRA-RED
middle
far
λ(μm) 2.5
3.3
5.0
10.0
40.0
300.0
ῡ(cm⁻¹) 4000
3000
2000
1000
250
33
Stretching modes
Lattice modes
-C-H
=C
H
≡C-H
C≡O
-C≡C-
-C≡N
C=C
C=O
C=N
N=O
-C-C-
-C-O-
-C-N
N-H
-O-H
Bending modes
(O=C=O)
(N≡N=O)

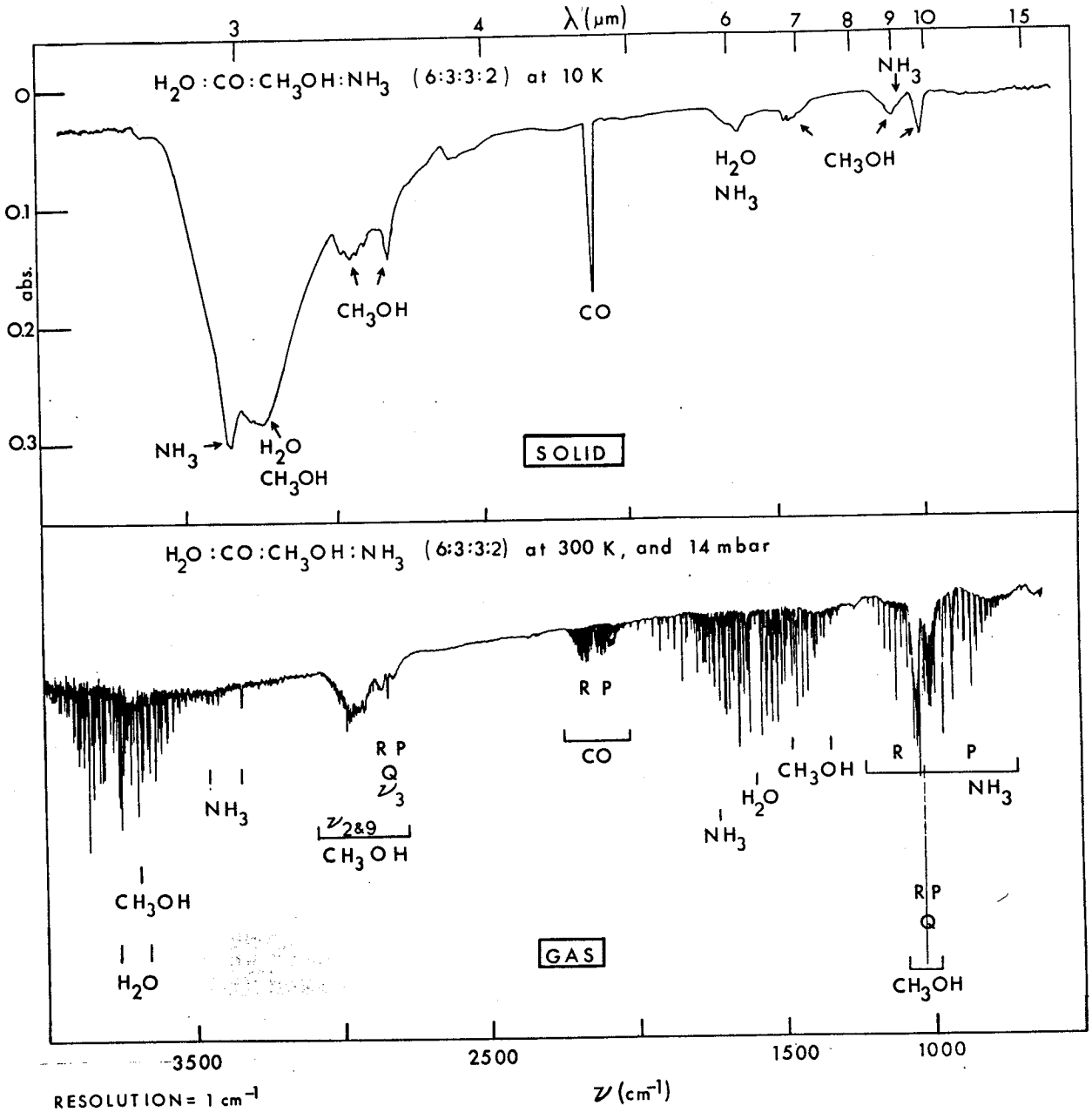
λ (μm)
3
4
6
7
8
9
10
15
$H_2O:CO:CH_3OH:NH_3$ (6:3:3:2) at 10 K
0
0.1
0.2
0.3
abs.
NH_3
H_2O
CH_3OH
CH_3OH
CO
H_2O
NH_3
CH_3OH
NH_3
SOLID
$H_2O:CO:CH_3OH:NH_3$ (6:3:3:2) at 300 K, and 14 mbar
R P
CO
R P
Q
ν_3
$\nu_{2\&9}$
CH_3OH
NH_3
CH_3OH
H_2O
NH_3
CH_3OH
H_2O
NH_3
R
P
R P
Q
CH_3OH
GAS
3500
2500
1500
1000
ν (cm^{-1})
RESOLUTION = 1 cm^{-1}

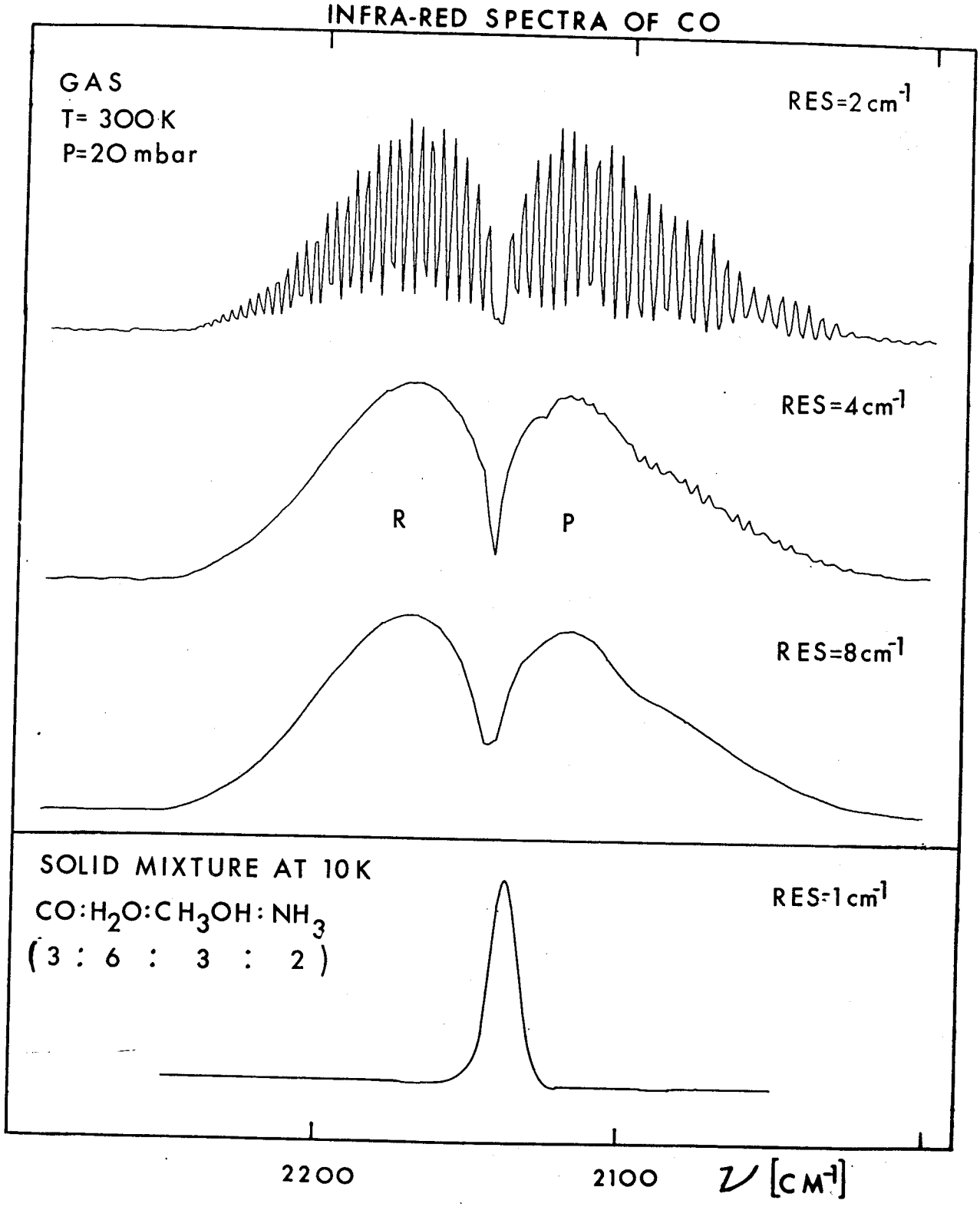
INFRA-RED SPECTRA OF CO
GAS
T= 300 K
P=20 mbar
RES=2 cm-1
RES=4 cm-1
R
P
RES=8 cm-1
SOLID MIXTURE AT 10 K
CO:H2O:CH3OH:NH3
(3 : 6 : 3 : 2)
RES=1 cm-1
2200
2100
ν [CM-1]

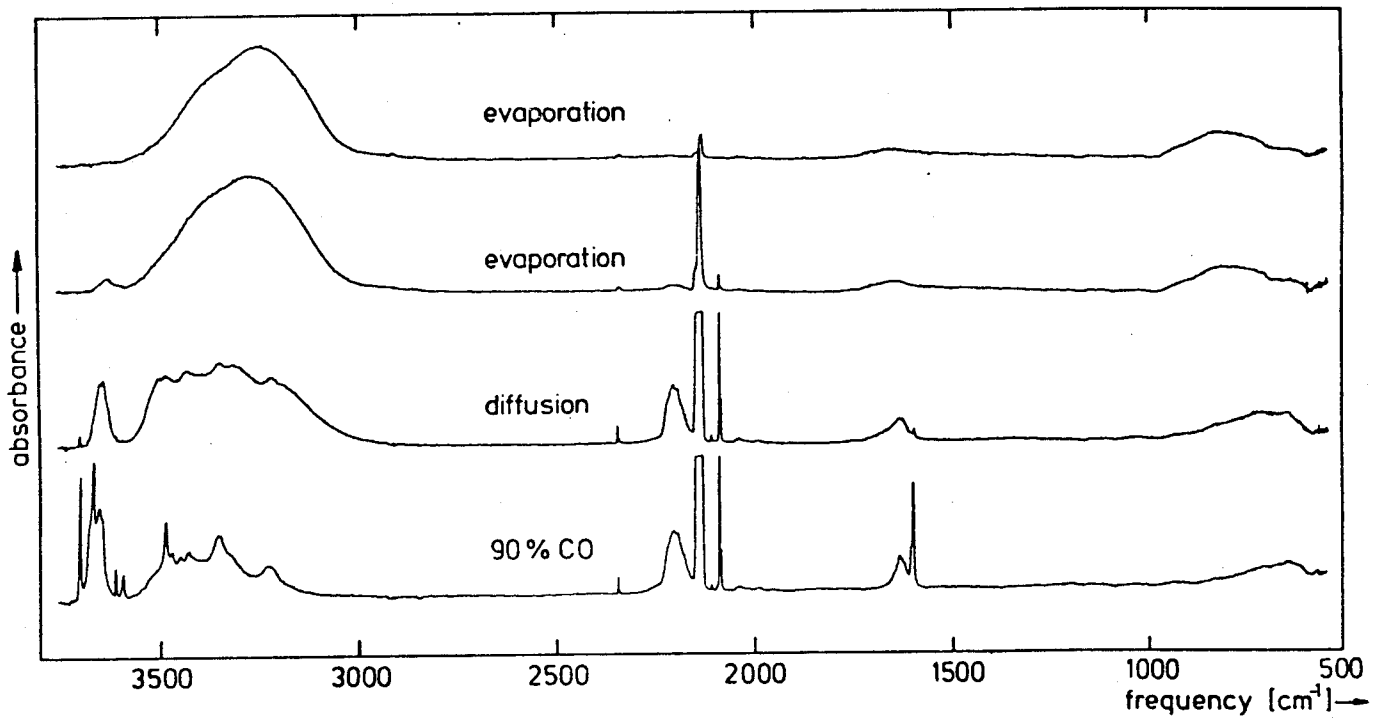
evaporation
evaporation
diffusion
90 % CO
absorbance
3500
3000
2500
2000
1500
1000
500
frequency [cm⁻¹]

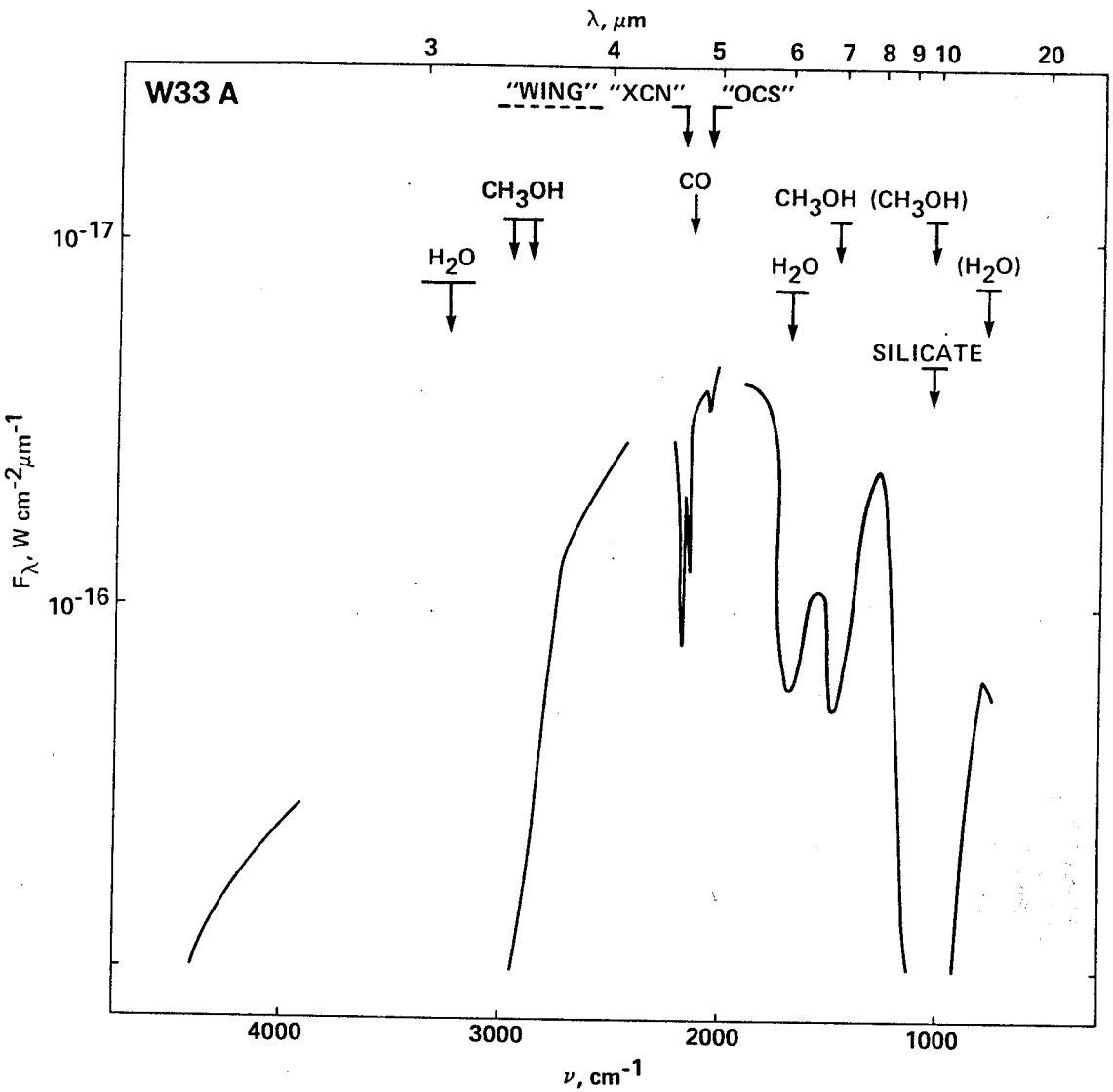
λ, μm
3
4
5
6
7
8
9
10
20
W33 A
"WING"
"XCN"
"OCS"
CO
CH3OH
CH3OH
(CH3OH)
H2O
H2O
(H2O)
SILICATE
10-17
10-16
Fλ, W cm-2μm-1
4000
3000
2000
1000
ν, cm-1

BAAS et al. (1988)

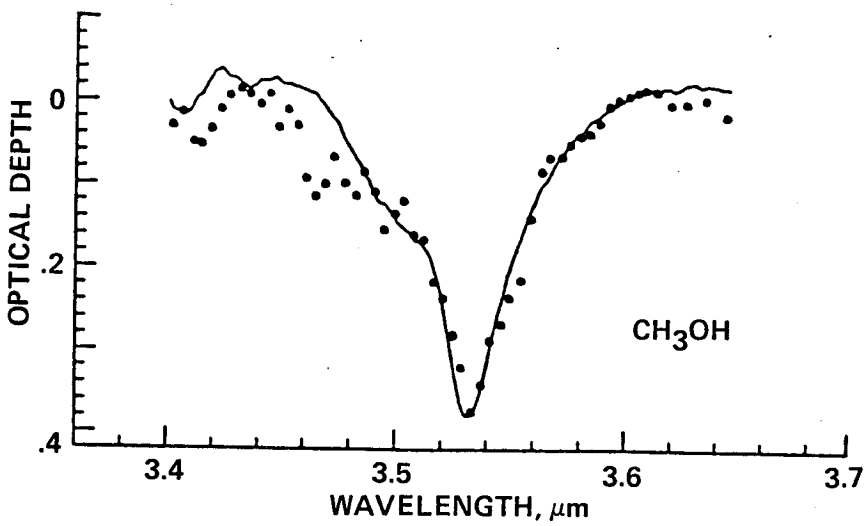

TIELENS

12

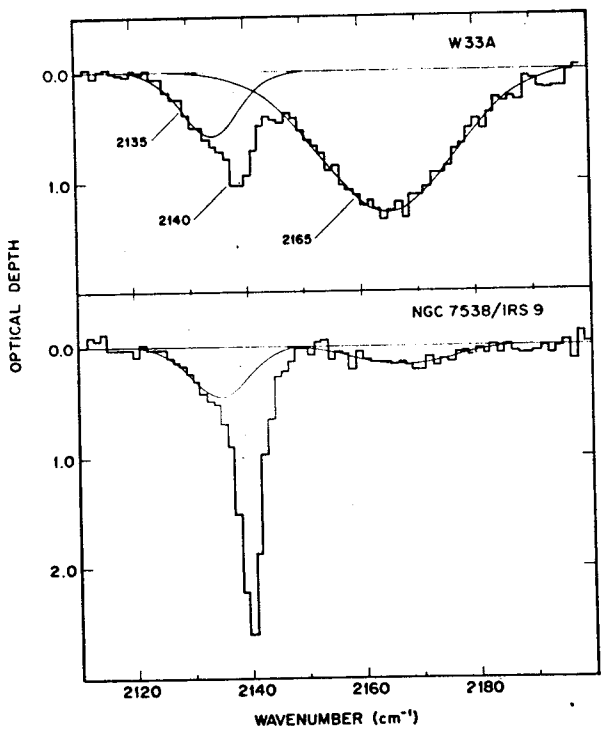
W33A
0.0
1.0
2135
2140
2165
NGC 7538/IRS 9
0.0
1.0
2.0
OPTICAL DEPTH
2120
2140
2160
2180
WAVENUMBER (cm⁻¹)

THE SOLID CO BAND PROFILE FOR CO IN DIFFERENT ICES

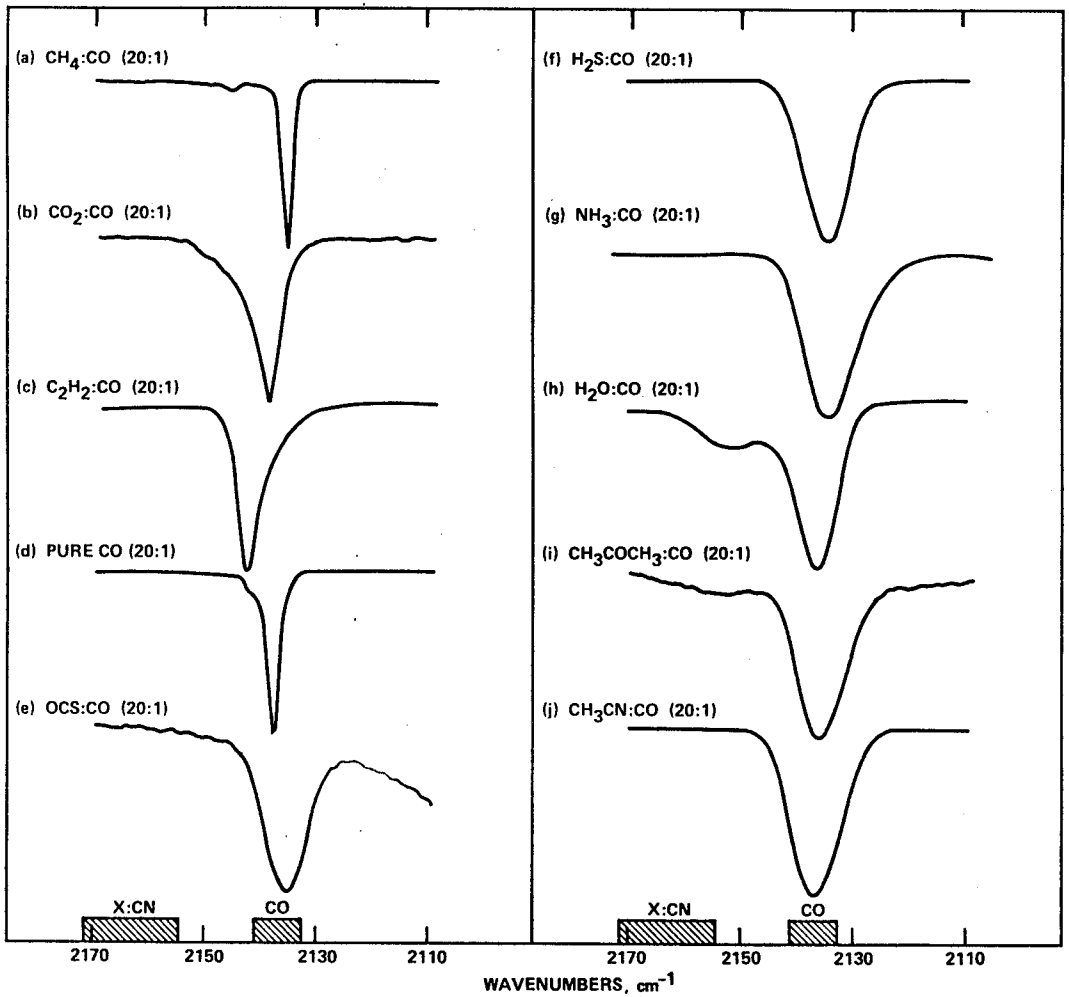

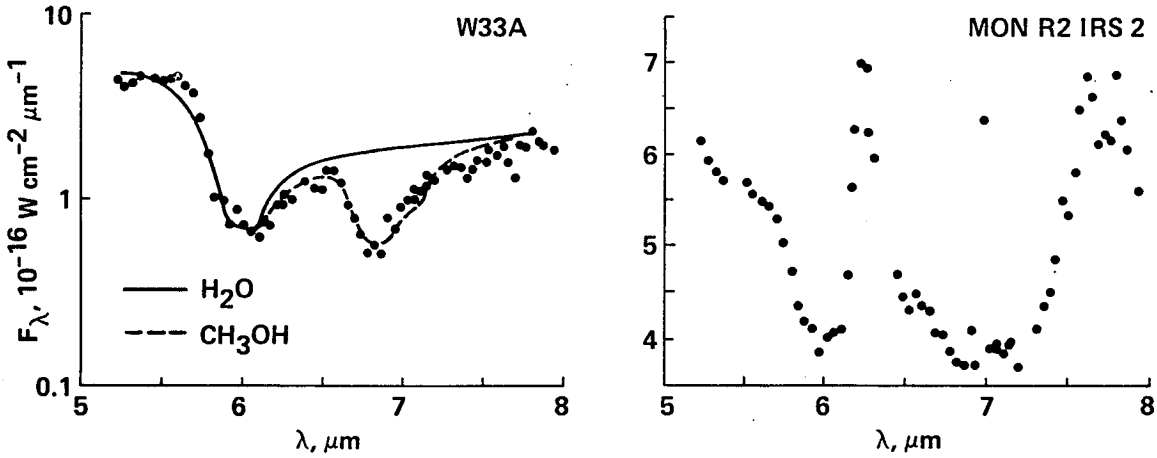
W33A
MON R2 IRS 2
10
1
0.1
7
6
5
4
5
6
7
8
F_λ, 10^{-16} W cm^{-2} μm^{-1}
λ, μm
H_2O
CH_3OH